

Accepted Manuscript

Title: Towards biomimics of cell membranes: Structural effect of Phosphatidylinositol triphosphate (PIP₃) on a lipid bilayer

Authors: Alessandra Luchini, Achebe N.O. Nzulumike, Tania K. Lind, Tommy Nylander, Robert Barker, Lise Arleth, Kell Mortensen, Marité Cardenas



PII: S0927-7765(18)30642-8
DOI: <https://doi.org/10.1016/j.colsurfb.2018.09.031>
Reference: COLSUB 9633

To appear in: *Colloids and Surfaces B: Biointerfaces*

Received date: 27-3-2018
Revised date: 31-8-2018
Accepted date: 13-9-2018

Please cite this article as: Luchini A, Nzulumike ANO, Lind TK, Nylander T, Barker R, Arleth L, Mortensen K, Cardenas M, Towards biomimics of cell membranes: Structural effect of Phosphatidylinositol triphosphate (PIP₃) on a lipid bilayer, *Colloids and Surfaces B: Biointerfaces* (2018), <https://doi.org/10.1016/j.colsurfb.2018.09.031>

This is a PDF file of an unedited manuscript that has been accepted for publication. As a service to our customers we are providing this early version of the manuscript. The manuscript will undergo copyediting, typesetting, and review of the resulting proof before it is published in its final form. Please note that during the production process errors may be discovered which could affect the content, and all legal disclaimers that apply to the journal pertain.

Towards biomimics of cell membranes: structural effect of Phosphatidylinositol triphosphate (PIP₃) on a lipid bilayer.

Alessandra Luchini ^a, Achebe N. O. Nzulumike ^a, Tania K. Lind ^b, Tommy Nylander ^c, Robert Barker ^d, Lise Arleth ^a, Kell Mortensen ^a and Marité Cardenas ^{c*}

^a Niels Bohr Institute, University of Copenhagen, Universitetsparken 5, 2100 Copenhagen, Denmark.

^bNano-Science Center and Institute of Chemistry, Copenhagen University, Universitetsparken 5, 2100 Copenhagen, Denmark.

^c Biofilms Research Center for Biointerfaces and Department of Biomedical Science, Faculty of Health and Society, Malmö University, Per Albin Hanssons Väg 35, 214 32 Malmö, Sweden.

^d Physical Chemistry 1, Lund University, PO Box 124, 221 00 Lund, Sweden.

^e Institut Laue-Langevin, 71 Avenue des Martyrs, 38000, Grenoble, France; current address University of Kent, CT2 7NZ Canterbury, Kent, United Kingdom.

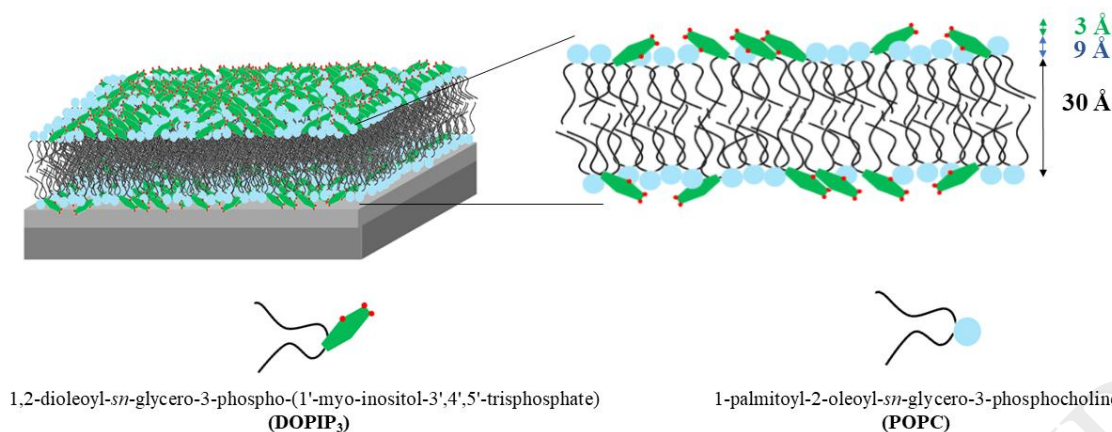
* corresponding author: marite.cardenas@mah.se

STATISTICAL SUMMARY

Total number of words:7252

Total number of figures/tables: 7

Graphical Abstract



Highlights:

- Supported lipid bilayer containing DOPIP₃ were characterized by surface sensitive techniques.
- Neutron Reflectometry revealed that POPC and DOPIP₃ form a symmetric bilayer.
- DOPIP₃ headgroups are not perpendicularly orientated with respect to the membrane surface
- DOPIP₃ headgroups have a preferred orientation close to the surrounding lipid headgroups.

Abstract

Phosphoinositide (PIP) lipids are anionic phospholipids playing a fundamental role for the activity of several transmembrane and soluble proteins. Among all, phosphoinositol-3',4',5'-trisphosphate (PIP₃) is a secondary signaling messenger that regulates the function of proteins involved in cell growth and gene transcription. The present study aims to reveal the structure of PIP-containing lipid membranes, which so far has been little explored. For this purpose, supported lipid bilayers (SLBs) containing 1,2-dioleoyl-*sn*-glycero-3-phospho-(1'-myo-inositol-3',4',5'-trisphosphate) (DOPIP₃) and 1-palmitoyl-2-oleoyl-*sn*-glycero-3-phosphocholine (POPC) were used as mimics of biomembranes. Surface sensitive techniques, i.e. Quartz Crystal Microbalance with Dissipation monitoring (QCM-D), Atomic Force Microscopy (AFM) and Neutron Reflectometry (NR), provided detailed information on the formation of SLB and the location of DOPIP₃ in the lipid membrane. Specifically, QCMD and AFM were used to identify the best condition for lipid deposition and to estimate the total bilayer thickness. On the other hand, NR was used to collect experimental structural data on the DOPIP₃ location and orientation within the lipid membrane.

The two bilayer leaflets showed the same DOPIP₃ concentration, thus suggesting the formation of a symmetric bilayer.

The headgroup layer thicknesses of the pure POPC and the mixed POPC/DOPIP₃ bilayer suggest that the DOPIP₃-headgroups have a preferred orientation, which is not perpendicular to the membrane surface, but instead it is close to the surrounding lipid headgroups. These results support the proposed PIP₃ tendency to interact with the other lipid headgroups as PC, so far exclusively suggested by MD simulations.

Keywords: Phosphoinositides, supported lipid bilayers, neutron reflectometry

1. Introduction

Anionic phospholipids are fundamental components of cellular membranes simultaneously participating at the membrane structure as well as at the regulation of several cellular processes through interaction with proteins and/or ions[1]. Phosphoinositide lipids (PIPs) are a class of anionic phospholipids, which act as primary or secondary messengers and thus allow for a fine regulation of many different signaling processes[2]. Typically, phosphoinositide lipids are produced by selective phosphorylation of phosphatidylinositol (PI). PI lipids are characterized by two acyl chains which are connected to the inositol ring by a phospho-glycerol unit. The inositol ring can be phosphorylated in position 3, 4 and 5, and its phosphorylation is regulated by the activity of specialized lipid kinases or phosphatases[3]. The phosphorylation of PI can result in seven different phosphatidylinositides[4].

Reversible PIP-production is fundamental to guarantee the high turnover needed for their regulatory activity; PI or PIP phosphorylation represents the first step in the signaling cascade in cells[5]. Indeed, PIPs regulate conformational changes of a large number of membrane-associated or transmembrane proteins. PIPs carry a negative charge at physiological pH, which is responsible for their interaction with basic protein regions[6, 7]. However, the interaction between cytosolic proteins and cytosolic protein domains also involves more selective recognition mechanisms[8]. Indeed, proteins are able to interact selectively with specific PIP species, which implies their ability to recognize PIPs according to their phosphorylated sites[9]. Due to their relevant biological functions including their involvement in severe pathologies, like cancer and diabetes, PIPs and specifically PIP-protein interactions have been intensively studied[8, 10-13]. The great majority of the published experimental studies available today

focuses on the interaction between PIPs and proteins using functional approaches. However, considerably less experimental data are available on the structure of PIP-containing lipid membranes despite this being a key pre-requisite to understand the molecular mechanisms behind specific interactions between proteins and PIPs. In particular, phosphatidylinositol-4,5-bisphosphate (PIP₂) and phosphatidylinositol-3,4,5-triphosphate (PIP₃) have been intensively studied as they are involved in several cellular functions such as cell growth, regulation of the actin cytoskeleton and gene transcription[2]. While PIP₂ is both a signaling molecule and a constituent of the plasma membrane (up to concentration ~2-5% mol/mol of all the plasma membrane lipids), PIP₃ is accumulated only in stimulated cells and acts as a second messenger being produced by PIP₂ phosphorylation[3].

Natural plasma membranes are composed by hundreds of lipid species, which makes it particularly difficult to extract detailed information on the molecular level from a physico-chemical point of view [1, 14]. Nevertheless, simpler model systems can be implemented to extract selective structural information on a few lipid species and probe their potential interaction within the membrane or with proteins. Today, most of the simpler models focus on the main mammalian lipid phosphatidylcholine (PC) and some charged species such as phosphatidylserine (PS) or phosphatidylglycerol (PG) and sterols[15-17]. In this context, supported lipid bilayers (SLBs), are particularly relevant as they provide a stable flat structure and a highly tuneable composition, which make them optimal candidates for many different kinds of experiments involving surface-sensitive techniques [18-20]. Due to their extensive implementation, detailed structural descriptions of SLBs are fundamental for the investigation of more complex systems, as those involving lipids and proteins[21-23].

Earlier, SLBs were implemented to test the formation of mixed membranes containing POPC and PIP₂ or PIP₃[24] and to probe their interaction with proteins[25], *e.g.* PIP₂-containing lipid membranes and Pleckstrin Homology-Phospholipase C-d1[25]. Specifically, kinetic information on the PIP-SLB formation mechanism was obtained by Quartz Crystal Microbalance with Dissipation Monitoring (QCM-D) and dual polarization interferometry [24] while some structural insights on PIP₂ or PIP₃ orientation in lipid bilayers were recently provided by Molecular Dynamics (MD)[26]. This is a particularly interesting approach to explore quite low PIP concentrations, though the MD results remain to be verified experimentally.

In the present project, SLBs are exploited to collect information on 1,2-dioleoyl-*sn*-glycero-3-phospho-(1'-myo-inositol-3',4',5'-triphosphate (DOPIP₃) and 1-palmitoyl-2-oleoyl-*sn*-glycero-3-phosphocholine (POPC) bilayers by means of QCM-D, Atomic Force Microscopy

(AFM) and Neutron Reflectometry (NR) measurements. SLBs were prepared by the vesicle-fusion method[20] with pure POPC or POPC/DOPIP₃ 90/10 mol/mol vesicles. The successful formation of SLBs was initially confirmed and monitored by QCM-D. AFM was subsequently implemented to obtain first structural insight such as bilayer thickness and their structure was subsequently characterized by NR. In particular by exploiting the intrinsic capability of neutrons to distinguish the two hydrogen isotopes[27], protium (H) and deuterium (D), the present characterization aimed at quantifying and locating PIP₃ in SLBs prepared with single chain deuterated POPC. To the best of our knowledge, NR data on PC/PIP₃ SLBs are presented here for the first time and provide new insight on the structure of PIP-containing bilayers. In particular, the reported data provide experimental evidence that the DOPIP₃ headgroup location is close to the membrane surface in spite of the larger volume compared to the other lipid headgroups. A detailed structural description of PC/PIP₃ SLB is needed in order to adopt this kind of lipid bilayer as a model system to reveal the nature of the interaction with specific proteins or protein domains. At the same time, the discussed results provide a relevant example of how the interaction between lipid headgroups can determine membrane structure.

2. Experimental Section

2.1 Materials

POPC (in the following renamed to hPOPC, $\geq 99\%$ purity), 1-palmitoyl-d31-2-oleoyl-*sn*-glycero-3-phosphocholine (dPOPC, $\geq 99\%$ purity) and DOPIP₃ ($\geq 99\%$ purity) were purchased from Avanti Polar Lipids, Inc. (Alabaster, AL) and used without further purification (Figure S1.1). 4-(2-hydroxyethyl)piperazine-1-ethanesulfonic acid (HEPES, $\geq 99.5\%$ purity), sodium chloride (NaCl, $\geq 99\%$ purity), ethylenediaminetetraacetic acid (EDTA, $\geq 99\%$ purity), heavy water (D₂O 99.9% purity), chloroform ($\geq 99.5\%$ purity), ethanol (98% purity), methanol (99.8% purity), hydrogen peroxide solution 30% w/w, sulfuric acid (H₂SO₄, 98% purity), and sodium dodecyl sulfate (SDS, $\geq 98.5\%$ purity) were purchased from Sigma-Aldrich Corp. Ultrapure Milli-Q (MQ) water with resistivity of 18.2 M Ω ·cm at 25 °C was used for all cleaning procedures, and preparation of all hydrogenated samples and buffers. SDS 5 % was used for cleaning QCM-D sensor crystals, and Hellmanex 2% (Hellma GmbH & Co., Germany) for any other cleaning.

2.2 Small Unilamellar Vesicle (SUV) Preparation

Lipids were dissolved in CHCl_3 (POPC) or 65:35 CHCl_3 : CH_3OH (DOPIP₃), mixed according to desired membrane composition (90/10 mol/mol respectively), dried under gentle nitrogen flow, and placed in vacuum overnight to ensure evaporation of all solvent. The resulting lipid films were rehydrated at room temperature for 1 h in MQ, and vortexed to fully suspend vesicles. Immediately before use for SLB formation, the suspension was diluted in buffer (20 mM HEPES, 200 mM NaCl, 1 mM EDTA, pH 7.5), tip sonicated for 5 min at pulses of 5 s on/off to consistently produce a clear solution of fusogenic SUVs, and loaded at a final concentration of 0.01 mg/mL in the case of QCMD and AFM measurement while a final concentration of 0.1 mg/mL was used for NR. Room temperature was maintained throughout preparation.

2.3 Quartz Crystal Microbalance with Dissipation Monitoring

QCM-D was performed with a Q-Sense E4 instrument (Q-Sense, Biolin Scientific AB, Sweden), using SiO_2 -coated 5 MHz quartz sensors. Crystals and O-rings were placed in Hellmanex 2% for 10 min, extensively flushed with absolute ethanol and MQ, and then dried under nitrogen flow. Immediately before use, the crystals were treated with a UV ozone cleaner (BioForce Nanosciences, Inc., Ames, IA) for 10 min. Before acquisition, the fundamental frequency and six overtones (3rd, 5th, 7th, 11th and 13th) were recorded and the system was equilibrated in MQ at 25 °C, until stable baselines were obtained. After equilibration in buffer (Figure 3, region I), 0.01 mg/mL SUVs were introduced in the flow cell at 0.1 mL/min and the typical signals for SLB fusion were followed (Figure 3, region II) until successful bilayer formation was complete (Figure 3, region III).

For homogeneous thin and rigid films fully coupled to the sensor surface, the recorded frequency shifts, normalized to the overtone number, can be simply related to the absorbed mass (Δm) through the Sauerbrey equation (equation 1), where C is the mass sensitivity constant corresponding to $17.7 \text{ ng}\cdot\text{cm}^2\cdot\text{Hz}^{-1}$ for the sensors used in this experiment.[28]

$$\frac{\Delta F_n}{n} = -\frac{1}{C} \Delta m \quad (1)$$

During the experiments, real-time shifts in the resonance frequency (ΔF_n) with respect to the calibration value were measured for different overtones indicated as F_n , with n representing the overtone number ($n=3, 5, 7, 9, 11, 13$). Simultaneously, also the energy dissipation factor (D) was evaluated for all the overtones[29].

2.4 Atomic Force Microscopy (AFM)

Atomic force microscopy measurements were carried out on a Nanoscope IV multimode AFM (Veeco Instruments Inc.). Images were generated in the PeakForce QNM (quantitative nanomechanical property mapping) mode with a silicon oxide tip (Olympus microcantilever OTR8 PS-W) with a spring constant of 0.15 N/m and a radius of curvature <20 nm. A freshly cleaved mica surface was imaged in ultrapure water to ensure a clean and smooth surface (RMS < 500 pm) prior to SLB formation. AFM imaging of the bilayer formation process was carried out under continuous flow of the vesicle solution at room temperature as described previously[20] using a slow gravity-fed flow of approximately 50 $\mu\text{L}/\text{min}$. After bilayer formation in ultrapure water, the membranes were rinsed with buffer. All images were recorded at a resolution of 512×512 pixels and with a scan rate of 1 Hz. The z-set point and differential gains were optimized during each scan. Images were analyzed and processed in the Gwyddion 2.22 software.

2.5 Neutron Reflectometry (NR) experiments

NR experiments were performed on FIGARO[30, 31] and D17[32] reflectometers at Institut Laue Langevin (ILL), Grenoble (France). FIGARO is a horizontal time of flight reflectometers, whereas D17 is a vertical reflectometer which was also used in the time of flight mode. On both instruments, two incoming angles (θ) typically of 0.8° and 3.2° were used to cover the q -range $8 \cdot 10^{-3} \text{ \AA}^{-1} < q < 0.25 \text{ \AA}^{-1}$, where q is defined as follows:

$$q = \frac{4\pi}{\lambda} \sin(\theta) \quad (2)$$

The measured reflected intensity ($I(q)$) was converted in an absolute reflectivity scale ($R(q)$) by normalization to the direct beam (I_0) measured at the same slit settings. Slits were chosen to vary with the incident angle in such a way as to provide a constant illumination of the sample (35×65 mm). The background was accounted for by using the average value from the regions of interest on both sides of the specular reflected beam and subtracted from the collected NR curve.

$$R(q) = \frac{I(q)}{I_0} \quad (3)$$

The main goal of the NR experiments is to reveal the scattering length density profile ($\rho(z)$) from the experimentally determined reflectivity profiles (equation 4). This gives information on the composition of the sample along the surface normal (z)[31, 33].

$$\rho = \sum_i \frac{n_i b_i}{V_m} \quad (4)$$

As reported in equation 4, ρ depends on the chemical and isotopic composition of the sample as the neutrons are sensitive to the nuclei composing the atoms in the molecules, where n_i is the number of atom i , b_i is the coherent scattering length, and V_m is the partial specific molecular volume (hereafter also referred as molecular volume).

NR was performed using custom-made solid/liquid flow cells with polished silicon crystals (111) with a surface area of 6 x 8 cm. Neutron cell flow modules and O-rings were cleaned by 3 cycles of 10 min bath sonication in 2%(vol/vol) Hellmanex and rinsing with MQ, followed by 3 cycles of 10 min bath sonication in MQ and rinsing with MQ. The crystals were rinsed with ethanol until surfaces were perfectly clear, soaked in detergent for 15 min, and cleaned with dilute piranha solution; 1:4:5 H₂O₂:H₂SO₄:H₂O at 80 °C for 15 min. Each step was followed by thorough rinsing with MQ to clean crystals and confirm hydrophilicity of surfaces. Finally, the crystals were treated with UV/ozone cleaner for 10 min before neutron cell assembly.

The temperature was maintained at 25 °C by circulating water from a thermostated water bath. Variation of the aqueous solvent contrast was achieved by exchanging the bulk solvent using an HPLC pump set to a flow rate of 1mL/min. Substrate surfaces were characterized in H₂O and D₂O, followed by slow manual syringe injection of SUVs and incubation for 1 h to allow for SLB formation. The membranes were characterized in at least 3 isotopic solvent contrasts, i.e. buffer with different ratio of D₂O to H₂O. In particular the buffers used during the experiments were prepared with pure D₂O (d-buffer, $\rho = 6.35 \cdot 10^{-6} \text{ \AA}^{-2}$), D₂O:H₂O 68:32 w/w (4 Matched Water, 4MW-buffer, $\rho = 4 \cdot 10^{-6} \text{ \AA}^{-2}$), D₂O:H₂O 52:48 (3 Matched Water, 3MW-buffer, $\rho = 3 \cdot 10^{-6} \text{ \AA}^{-2}$), D₂O:H₂O 38:62 w/w (Silicon Matched Water, SMW-buffer $\rho = 2.07 \cdot 10^{-6} \text{ \AA}^{-2}$) and pure H₂O buffer (h-buffer, $\rho = -0.56 \cdot 10^{-6} \text{ \AA}^{-2}$).

2.6 NR data analysis

NR data were analysed with RasCAL[34]. In this software environment, the interface between the substrate and the bulk is considered as a stratified medium composed by different slabs. The reflectivity originating from such an interface can be described according to the optical matrix method[35], where each of the slabs included in the model is characterized by four output parameters: thickness (t), ρ , the surface coverage expressed as the volume fraction of the molecules deposited on the substrate (ϕ) and the roughness (σ).

SLBs were treated as composed by two external slabs (the lipid headgroups) and one or two intermediate slabs to describe the lipid acyl chains (tails) in each leaflet. An additional slab was

used to describe the substrate surface in terms of its natural silicon oxide layer, whereas the silicon and the solvent were considered as bulk on the two sides of the sample.

The experimental data were analyzed by creating a custom model within RasCAL which allows for defining custom fitting parameters that can be directly optimized to the experimental data. In the present case, Figure S1.2 illustrates the chosen fitting parameters and how they can be related to the standard output parameters.

Among the fitting parameters, the area per lipid (A_{lip}) was adopted to impose molecular constraints between the tails and the headgroups belonging to the same leaflet, as already reported elsewhere[18, 36, 37] (see also Supplementary Material). Furthermore, in the case of POPC/DOPIP₃ SLBs, the lipid molar fraction was explicitly taken into account among the fitting parameters. The molecular volumes of the headgroups and tails (V_n^{dry} and V_t^{dry}) were as well directly optimized to the experimental. Indeed, the scattering length, $B = \sum_i n_i b_i$, is a quantity that can be calculated from the chemical and isotopic composition of the lipids (see Table S1.1). In case of DOPIP₃ headgroup, B was calculated by taking into account the potential exchange of the labile hydrogen atoms with the hydrogen atoms in the solvent. On the other hand, the molecular volumes can be reasonably estimated from already reported experimental or simulation data[38]. By choosing the molecular volume as a fitting parameter, the atomic composition of the molecules is kept constant while the volume that they occupy is allowed to vary (in response to the surrounding environment) to give the best ρ value according to the experimental data. Indeed, while accurate values for the lipid molecular volumes can be obtained both theoretically and experimentally in the case of pure lipid bilayers (composed by a single lipid species) less information is available in the literature about molecular volumes for multicomponent lipid bilayers and more specifically for PIPs/PC lipid bilayers. This is due to the fact that the lipid molecular volume can vary according to the composition of a specific bilayer both in terms of number of lipid species and their relative abundance. In the present case, it is worth mentioning that only variations within 4% for the headgroups and for the tails of the initial guess for POPC / DOPIP₃ volumes (see Table S1.2) were observed during data fitting. The initial guess was based on the already reported value for the POPC molecular volume[39] and the DOPIP₃ molecular volume which was calculated from the molecular structure of the lipid.

The experimental curves collected for the same lipid bilayer exposed to the different solvents were simultaneously analysed with the same model. This approach, known as global analysis, gives significantly reduced ambiguity in the interpretation of the sample structure due to the

different sensitivity that the curves collected in the different solvents exhibit with respect to the different sample components[40]. Indeed, the buffers with high D₂O content, *i.e.* d-buffer and 4MW-buffer, exhibit high contrast (difference in ρ between the solvent and the sample) for the h-lipid acyl chains, which are characterized by negative ρ . On the other hand, the buffers with high H₂O content, *i.e.* SMW and h-buffer, exhibit high contrast for the lipid headgroups and the d-acyl chains. In addition, SMW-buffer perfectly mask the signal coming from the silicon bulk, so that only the signal arising from the silicon oxide layer and the lipid bilayer is detected in this solvent.

To further constrain the generated model to the maximum number of experimental data sets, curves collected for the samples prepared with hPOPC and dPOPC were simultaneously fitted. Indeed, hPOPC and dPOPC have the same molecular structure and thus produce only variation in the ρ of the bilayer. Hence the data collected for the bilayers with hPOPC and dPOPC can be constrained to have the same structures but different B as input (see Table S1.1). Furthermore, the dPOPC used in this study is only partially tail deuterated in the tail region, thus only the ρ of the acyl chain layer become affected.

During the experiments, bare silicon crystals were initially characterized to evaluate the structure of the native silicon oxide (see section S3 in Supplementary Material). Subsequently SLBs were formed on the support surface. During data analysis, the output parameters for the corresponding substrate were kept fixed to the values determined in their preliminary characterization.

3. Results and Discussions

3.1. QCM-D Measurements

SLB formation by vesicle fusion was initially verified by QCM-D measurements. Figure 1 shows the formation of hPOPC and hPOPC/DOPIP₃ bilayers by monitoring ΔF and ΔD over time, see also Figure S2.1 and S2.2. In particular, the injection of vesicles induces a fast decrease in ΔF and parallel increase in ΔD (region II), which are produced by vesicle adsorption on the substrate surface. As already reported for vesicle-fusion in the presence of salts [41], once a critical concentration of adsorbed vesicles is reached at the sensor surface (ΔF minimum and ΔD maximum in region II), the vesicles will start to fuse and form a flat lipid bilayer. As the vesicles contain a large amount of water, a mass decrease (an increase in ΔF), is expected when they fuse to form the lipid bilayer. In parallel, ΔD is expected to decrease

as the lipid bilayer present a more rigid structure with respect to adsorbed vesicles. In the present case, the effective formation of a lipid bilayer with high surface coverage was confirmed by the final ΔF value ~ -26 Hz and a corresponding dissipation factor decrease to a value close to 0.

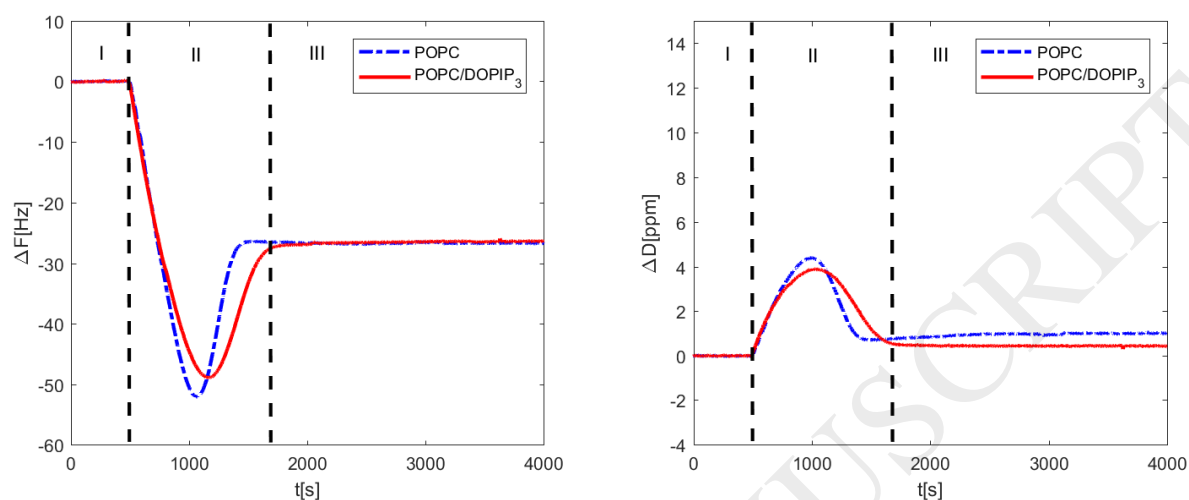


Figure 1 - QCM-D data monitoring the formation of hPOPC (blue) and hPOPC/DOPIP₃ (red) lipid bilayers; frequency (ΔF) and dissipation (ΔD) shifts for the sensor harmonics $n=5$ vs time (t), left and right panel respectively. Region I=equilibration of the sensor in buffer; region II=injection of lipid vesicles, adsorption on the sensor surface and fusion to form the SLB; Region III=complete SLB on the sensor surface.

While in the case of POPC, the formation of a lipid bilayer through vesicle fusion was expected, in the case of POPC/DOPIP₃ it was fundamental to verify that the presence of DOPIP₃, which has a considerably larger headgroup than POPC, did not prevent the SLB formation.

The presence of DOPIP₃ in the vesicles slowed down the adsorption process, and but still the following formation of the lipid bilayer was observed. This evidence is in agreement with the results of Baumann *et al.* [24], although the buffer composition and lipid concentration was different. Indeed, ΔF minimum and ΔD maximum were reached later in time with respect to the pure POPC sample. This observation can be related to the negative charge of PIP₃ at pH = 7.5[26], which slows down the vesicle adsorption on the negative quartz surface. Nevertheless, the lower vesicle adsorption rate did not affect the formation of the POPC/DOPIP₃ SLB.

Besides the observation of the SLB formation both in the case of POPC and POPC/DOPIP₃, the similar ΔF and ΔD value for POPC and POPC/DOPIP₃ bilayers (region III) suggests a similar lipid amount of adsorbed lipids. Indeed, although equation 1 refers to a rigid film ($\Delta D=0$), it still possible to use the equation 1 in the present case to make qualitative comparison between the two lipid systems. The absorbed mass resulted to be ~ 470 and ~ 460 ng/cm² for

POPC and POPC/DOPIP₃ respectively. These results are in good agreement with previously reported values for SLB formation on QCMD sensors.[42]

QCMD was used to identify the best condition for lipid deposition, however this technique can only provide information of lipid adsorption kinetics. For this reason, AFM and in particular NR resulted fundamental to complement the characterization of the SLBs with structural information.

3.2 AFM measurements

AFM measurements further validated the successful formation of SLBs by POPC/DOPIP₃ vesicle deposition and it was used to estimate the total bilayer thickness. *In situ* lipid deposition in the AFM measuring cell was performed three times and showed bilayers of high coverage and homogeneous in-plane lipid distribution once the vesicle fusion process had completed. The image in Figure 4 was recorded during the membrane formation process and shows an incomplete bilayer that allows for height measurements and calculation of statistical quantities. The average height and median height values of the image in Figure 2 were 4.6 ± 0.2 nm and 5.0 ± 0.2 nm, respectively. It was otherwise not possible to identify the height on full SLB as there were no detectable defects.

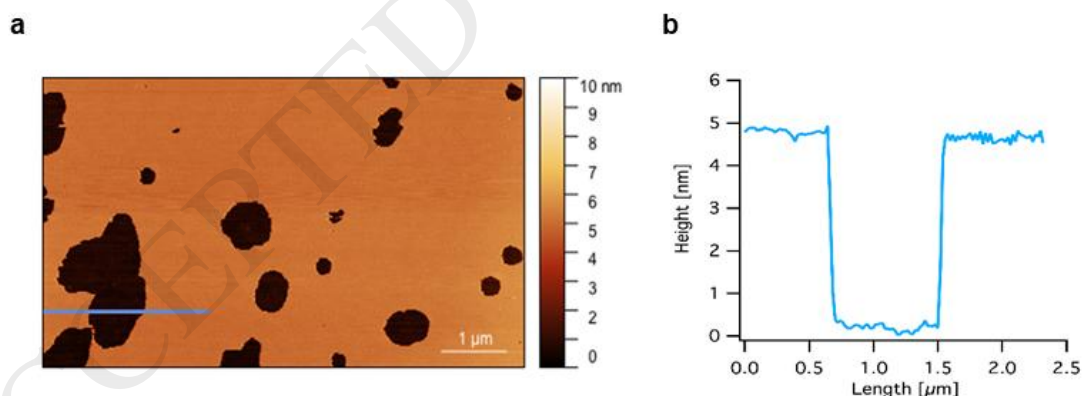


Figure 2 - Panel a: AFM image recorded during SLB formation from POPC/DOPIP₃ vesicle fusion on freshly cleaved mica. Panel b: line profile showing bilayer thickness from the edges of a defect as indicated by the blue line in panel a.

3.3 NR measurements

NR measurements were performed to reveal the SLB structure and highlight the effect of the presence of PIP₃ as well as its location within the membrane. NR data were collected for pure

hPOPC bilayer, which was used as the reference in this study. Figure 3 shows the experimental data together with the fitted curves and the SLD profiles obtained from data analysis.

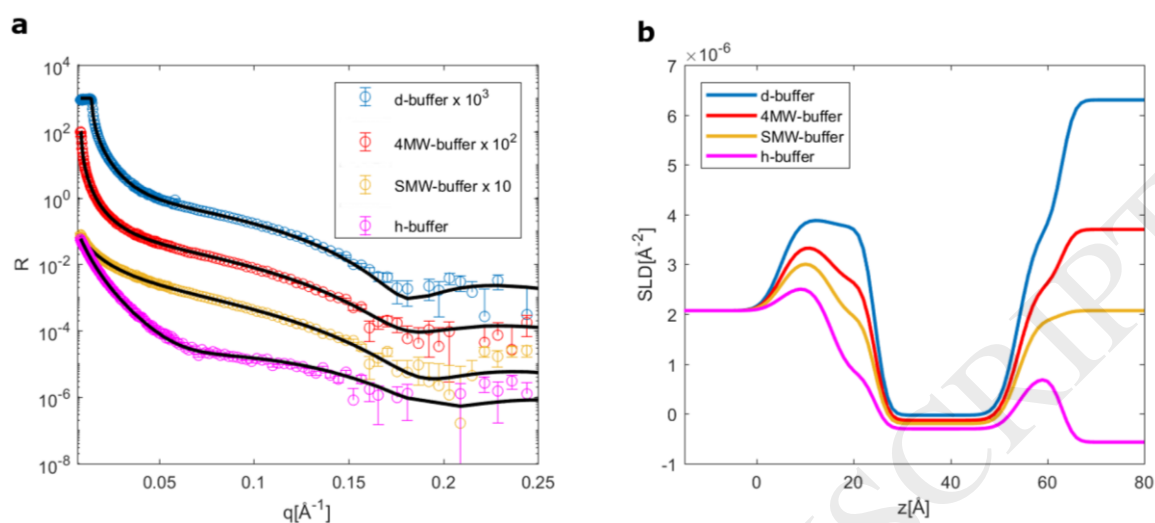


Figure 3 - NR data collected on FIGARO for hPOPC (panel a) bilayer in d-buffer, 4MW-buffer, SMW-buffer and h-buffer. The curves corresponding to the different solvents were offset for clarity, as reported in the legend. The SLD profiles obtained from the global optimization of the fitting parameters are given for hPOPC (panel b) and

The bilayer was described by the standard model including two outer layers accounting for the headgroups and one intermediate layer accounting for the tails of both leaflets. As the bilayer is composed by a single lipid species the two headgroup layers were constrained to the same fitting parameters.

The main structural parameters obtained from the data fitting (Table 1) are in good agreement with the expected structure of POPC bilayers as previously reported in the literature[43].

Figure 4 shows the NR data collected for the DOPIP₃-containing bilayers where, respectively, hPOPC and dPOPC were used. Indeed, it has been extensively demonstrated that selective deuteration of lipids is a very suitable method to vary the contrast between different sample components without affecting their structure[43-50]. In this case the first goal of the data analysis was to investigate the location of PIP₃ within the lipid bilayer, *i.e.* if it distributed symmetrically or asymmetrically between the two leaflets. The DOPIP₃ headgroup has a considerably different scattering length with respect to POPC (see Table S1.1). However, by replacing hPOPC with dPOPC, an even more significant contrast (difference in scattering length density) was achieved also between the PIP₃ and POPC tails (see Table S1.1).

As for POPC bilayers, the data sets for hPOPC/DOPIP₃ and dPOPC/DOPIP₃ were initially analyzed separately and the fit analysis converged to similar parameter values. Therefore, the

two data sets were simultaneously analysed instead. The adopted model imposed the same lipid structural parameters but using the relevant scattering lengths for hPOPC and dPOPC tails and allowing the fitting curves for the two data sets to reflect different coverage for the two bilayers. During the preliminary data analysis, a more complex model was used, where the bilayer was described by 4 layers accounting for the tails and headgroups of each of the two leaflets. In this case, molecular constraints were applied only between the headgroups and the tails belonging to the same leaflet; this allowed for investigating the the distribution of DOPIP₃ between the two bilayer leaflets. As it turned out, the obtained values for the fitting parameters highlighted that upon addition of DOPIP₃ the bilayer leaflets were still characterized by a symmetric composition, *i.e.* DOPIP₃ is symmetrically distributed in the two bilayer leaflets (in Supplementary Materials simulated curves corresponding to asymmetric distribution of DOPIP₃ are reported for comparison with the adopted model). Consequently, the data analysis was refined by applying constraints between the two leaflets in order to reduce the number of fitting parameters; the headgroup layers were constrained to the same fitting parameters (inner and outer headgroups are alike) and a single intermediate layer was used for the tails.

As reported in Table 1, the presence of DOPIP₃ in the bilayer did not significantly affect the the bilayer structure as compared to the pure POPC SLB; it mainly produced a small increment in the headgroup layer thickness (the effect of the headgroup layer thickness on the theoretical NR curves is reported in Supplementary Material).

The distance between the first DOPIP₃ phosphate group (close to the glycerol unit) and the most external phosphate on the inositol ring (position 4) is $\sim 5 \text{ \AA}$ [26]. The first phosphate group is very close to the phosphate groups of the surrounding PC headgroups; in this situation, the DOPIP₃ headgroup would protrude $\sim 4 \text{ \AA}$ out from the membrane if it undertook a perpendicular orientation with respect to the membrane surface [51].

Indeed, MD simulation performed by Wu and co-workers [26] showed that the orientation of the DOPIP₃ headgroup was influenced not only by solvation but also by the formation of hydrogen bonds with the surrounding headgroups. Particularly, these latter would stabilize the DOPIP₃ headgroup tilting towards the membrane surface with a mean angle $\sim 40^\circ$ [52].

However it should be remembered that MD simulations are performed using 1) a reduced number of lipids in order for the molecules to be explicitly taken into account (being in some case limited event to a single PIP₃ molecule in the bilayer[26]) and 2) limited simulation time. These restrictions can impact the statistical relevance of the results. From this point of view NR can highly complement MD studies providing experimental data averaged on a large

number of lipids. At the same time, the analysis of NR results can be reinforced by the great molecular detail provided by the MD structure. In the present case, the thickness increment of $(3 \pm 2) \text{ \AA}$ produced by DOPIP₃ in POPC/DOPIP₃ bilayer suggests a broad distribution of orientations for the DOPIP₃ headgroups. Nevertheless, this distribution resulted to be centered on a value smaller than the expected one for a perpendicular orientation of the DOPIP₃ inositol ring, thus indicating a preferred orientation for the DOPIP₃ headgroup which is actually closer to the membrane surface and the surrounding lipid headgroups.

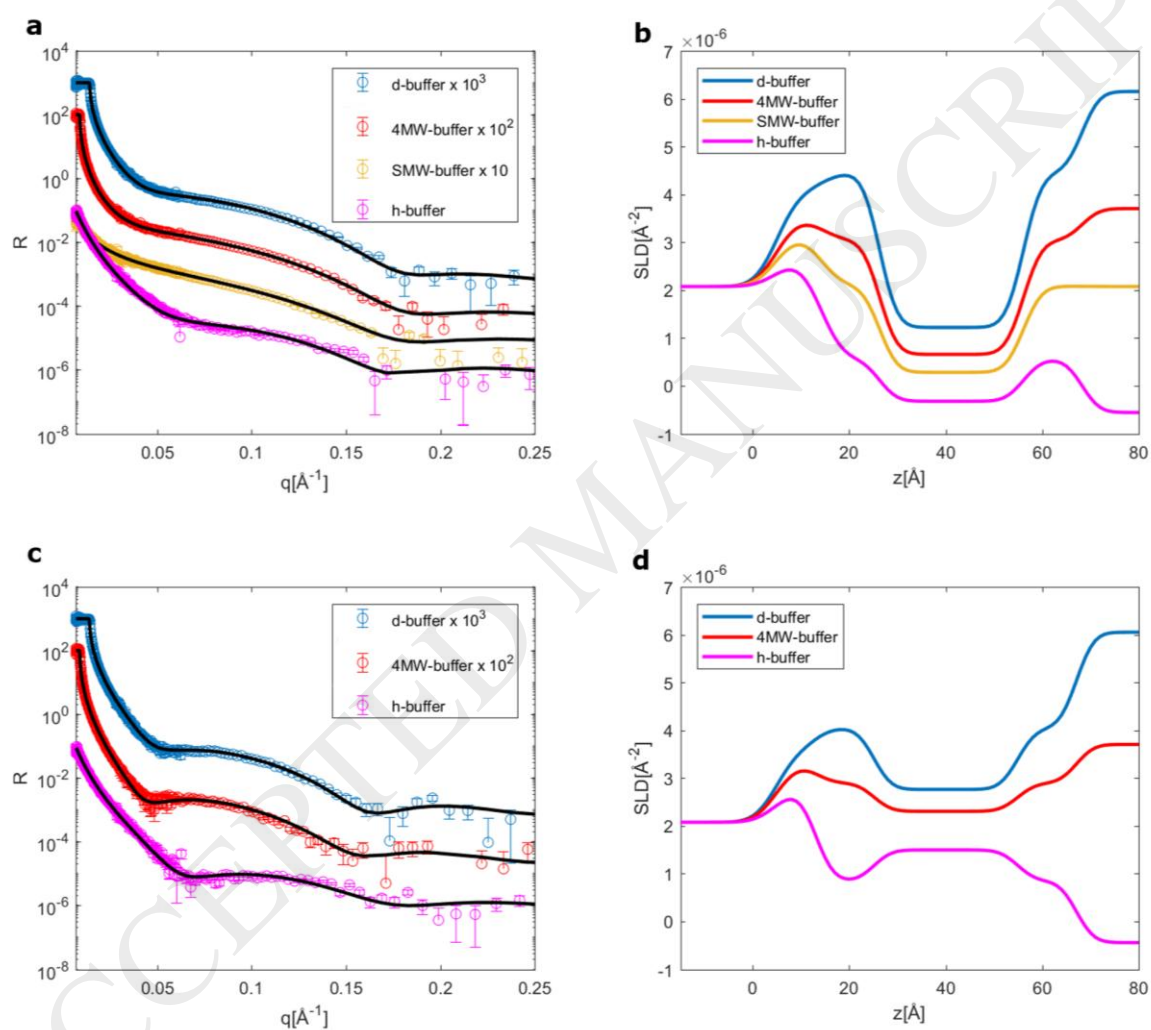


Figure 4 - NR data collected on D17 for hPOPC/DOPIP₃ (panel a) and dPOPC/DOPIP₃ (panel c) bilayers in d-buffer, 4MW-buffer, SMW-buffer and h-buffer. The curves corresponding to the different solvents were offset for clarity, as reported in the legend. The SLD profiles obtained from the optimization of the fitting parameters is reported for hPOPC/DOPIP₃ (panel b) and dPOPC/DOPIP₃ (panel d). Data collected for hPOPC/DOPIP₃ (panel a) and dPOPC/DOPIP₃ (panel c) bilayer were simultaneously fitted by the same model.

The calculated value for the area-per-lipid, A_{lip} , for hPOPC and hPOPC/DOPIP₃ (Table 1) indicates that the surface area associated to each lipid is only slightly affected by the presence of DOPIP₃.

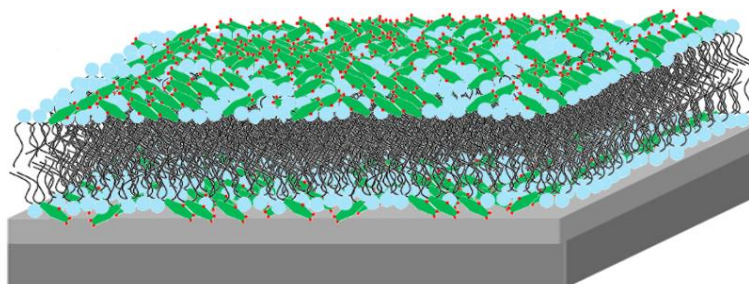


Figure 5 - Schematic representation of POPC/DOPIP₃. The DOPIP₃ headgroup closer to the membrane surface are reported in green with red dots representing the phosphorylated sites; POPC molecules are represented in blue.

Interestingly the composition of POPC/DOPIP₃ bilayers was considerably different from the nominal molar ratio of POPC and DOPIP₃ used to prepare the vesicles (*i.e.* 90/10 mol/mol). As reported in Table 1, NR data indicated that the molar ratio of POPC/DOPIP₃ in the characterized sample was 61/39 mol/mol. As already reported elsewhere[44, 53], SLBs formed by vesicle fusion can exhibit different composition with respect to the nominal sample composition due to heterogeneity in the lipid distribution among vesicles with broad size distribution. Fluorescence measurements performed on the single liposome level demonstrated that vesicles in suspension can exhibit a high degree of heterogeneity in their composition[54]. This compositional heterogeneity is associated to size polydispersity, *i.e.* small vesicles can exhibit a different composition with respect to large vesicles due to curvature effects and the formation of SLBs with different composition from the nominal can be promoted by the small vesicles reaching the substrate surface first [44]. These arguments explain the NR results of DOPIP₃ enrichment in the characterized SLBs. In particular, the experimental data suggests that the concentration of DOPIP₃ in smaller and more curved vesicles is higher than in larger less curved vesicles. Smaller vesicles diffuse faster on the substrate surface, thus producing higher DOPIP₃ concentration in the SLB than expected from the nominal concentration of the vesicles.

Table 1 - Structural parameters obtained from the fitting of NR data. A_{lip} = averaged area per lipid corrected for the lipid coverage; ρ_t =scattering length density of the tails; ρ_h =scattering length density of the headgroups (the exchange of the 5 labile hydrogen atoms in the headgroup was taken into

account); ϕ_t = tail surface coverage; ϕ_h = headgroup surface coverage; t_t =tail thickness; t_h = headgroup thickness. Thickness values were calculated according to equation S1.7.

Parameter	hPOPC	hPOPC/DOPIP ₃	dPOPC/DOPIP ₃
$A_{lip} [\text{Å}^2]$	62 ± 1	63 ± 3	
$\rho_t \cdot 10^{-6} [\text{Å}^{-2}]$	-0.29 ± 0.05	-0.26 ± 0.04	2.37 ± 0.02
$\rho_h \cdot 10^{-6} [\text{Å}^{-2}]$	1.82 ± 0.11	2.33 ± 0.25 (d-buffer) 2.21 ± 0.22 (4MW-buffer) 2.08 ± 0.20 (SMW-buffer) 1.93 ± 0.17 (h-buffer)	
ϕ_t	0.96 ± 0.01	0.77 ± 0.02	0.81 ± 0.03
ϕ_h	0.57 ± 0.02	0.49 ± 0.03	0.54 ± 0.04
$t_t [\text{Å}]$	30 ± 1	30 ± 1	
$t_h [\text{Å}]$	9 ± 1	12 ± 1	

4. Conclusions

PIPs are anionic phospholipids that play an important biological role as interaction partner of different proteins thus regulating several cellular processes[2]. In the view of exploring PIP-protein co-structure in lipid membranes, SLBs are a suitable system for the implementation of surface-sensitive techniques to study biomolecular interaction with and in biomembrane mimics. Here the structure and composition of SLBs composed of POPC and DOPIP₃ was discussed, providing, for the first time, experimental structural data by NR on this kind of SLB. Indeed, similar lipid bilayers were previously characterized by QCMD and MD. However, in the first case only the bilayer formation kinetics was investigated and in the second case the experimental validation of the simulation results was missing.

The best condition for lipid bilayer deposition were initially explored by means of QCMD measurements. AFM provided insights on the total bilayer thickness, while NR provided a detailed picture of the lipid bilayer structures.

As a result, the overall SLB structural properties are only slightly affected by DOPIP₃; the tail organization appeared to be unperturbed and a small increment of the headgroup thickness was observed with respect to the pure POPC bilayer. Among the different orientation that the DOPIP₃ headgroup can undertake, NR results suggest a preferred orientation, which is actually in the proximity of the membrane surface. This observation suggests that the DOPIP₃ headgroups have a preferred orientation in the proximity of the other lipid headgroups, Concerning the SLB composition, PIP₃ was symmetrically distributed between the two leaflets, although its concentration was significantly higher than the nominal composition of the vesicle preparation (39 % mol/mol compared to 10% mol/mol, respectively). Discrepancies between the nominal and the experimental composition of SLBs formed by vesicle fusion are well documented[44, 53]. Indeed, the inhomogeneous composition of the vesicles (different sizes together with different distribution of the lipids in the vesicle populations) can be the determining factor for SLB composition. This is important information to consider when designing experiments with controlled PIP₃ composition in the bilayer to assess the specific interactions with proteins from solution.

Altogether, the present study provided valuable information on the structure of DOPIP₃-containing SLBs, which represent the fundamental scientific background for future studies aimed at exploiting surface-sensitive techniques to shed light on the interaction between PIPs and proteins. Indeed, the way the surrounding lipids can affect DOPIP₃ orientation may have a pivotal role in the recognition processes occurring at cellular membrane interfaces.

Acknowledgements

The authors thank the Institut Laue-Langevin for allocation of beamtime (doi :10.5291/ILL-DATA.9-13-453 and 10.5291/ILL-DATA.9-13-490). Danscatt for travel support and the Lundbeck Foundation Center for Biomembranes in Nano Medicine, Novo Nordisk foundation SYNERGY program and Interreg project ESS&MAXIV Cross Border Science and Society for funding (MAX4ESSFUN). MC thanks the Swedish Research Council for funding the project 2013-4171).

References

- [1] T. Kimura, W. Jennings, R.M. Epand, Roles of specific lipid species in the cell and their molecular mechanism, *Prog Lipid Res*, 62 (2016) 75-92.
- [2] G. Di Paolo, P. De Camilli, Phosphoinositides in cell regulation and membrane dynamics, *Nature*, 443 (2006) 651.
- [3] A. Toker, Phosphatidylinositol Bisphosphate and Trisphosphate, *Encyclopedia of Biological Chemistry*, 3 (2004).
- [4] K.F. Tolia, L.C. Cantley, Pathways for phosphoinositide synthesis, *Chem Phys Lipids*, 98 (1999) 69-77.

- [5] D.E. Logothetis, V.I. Petrou, M. Zhang, R. Mahajan, X.Y. Meng, S.K. Adney, M. Cui, L. Baki, Phosphoinositide Control of Membrane Protein Function: A Frontier Led by Studies on Ion Channels, *Annu Rev Physiol*, 77 (2015) 81-+.
- [6] M.P. Czech, PIP2 and PIP3: complex roles at the cell surface, *Cell*, 100 (2000) 603-606.
- [7] B.H. Falkenburger, J.B. Jensen, E.J. Dickson, B.C. Suh, B. Hille, Phosphoinositides: lipid regulators of membrane proteins, *J Physiol*, 588 (2010) 3179-3185.
- [8] S. McLaughlin, D. Murray, Plasma membrane phosphoinositide organization by protein electrostatics, *Nature*, 438 (2005) 605-611.
- [9] S.E. Lietzke, S. Bose, T. Cronin, J. Klarlund, A. Chawla, M.P. Czech, D.G. Lambright, Structural basis of 3-phosphoinositide recognition by pleckstrin homology domains, *Mol Cell*, 6 (2000) 385-394.
- [10] T. Maffucci, M. Falasca, Specificity in pleckstrin homology (PH) domain membrane targeting: a role for a phosphoinositide-protein co-operative mechanism, *FEBS Lett*, 506 (2001) 173-179.
- [11] M. Lenoir, I. Kufareva, R. Abagyan, M. Overduin, Membrane and Protein Interactions of the Pleckstrin Homology Domain Superfamily, *Membranes (Basel)*, 5 (2015) 646-663.
- [12] R.V. Stahelin, J.L. Scott, C.T. Frick, Cellular and molecular interactions of phosphoinositides and peripheral proteins, *Chem Phys Lipids*, 182 (2014) 3-18.
- [13] W. Cho, R.V. Stahelin, Membrane-protein interactions in cell signaling and membrane trafficking, *Annu Rev Biophys Biomol Struct*, 34 (2005) 119-151.
- [14] H.I. Ingólfsson, M.N. Melo, F.J. van Eerden, C. Arnarez, C.A. Lopez, T.A. Wassenaar, X. Periole, A.H. de Vries, D.P. Tieleman, S.J. Marrink, Lipid Organization of the Plasma Membrane, *Journal of the American Chemical Society*, 136 (2014) 14554-14559.
- [15] A. Martel, L. Antony, Y. Gerelli, L. Porcar, A. Fluitt, K. Hoffmann, I. Kiesel, M. Vivaudou, G. Fragneto, J.J. de Pablo, Membrane Permeation versus Amyloidogenicity: A Multitechnique Study of Islet Amyloid Polypeptide Interaction with Model Membranes, *Journal of the American Chemical Society*, 139 (2017) 137-148.
- [16] R.M. Verly, J.M. Resende, E.F.C. Junior, M.T.Q. de Magalhães, C.F.C.R. Guimarães, V.H.O. Munhoz, M.P. Bemquerer, F.C.L. Almeida, M.M. Santoro, D. Piló-Veloso, B. Bechinger, Structure and membrane interactions of the homodimeric antibiotic peptide homotarsinin, *Scientific Reports*, 7 (2017) 40854.
- [17] A. Melcrová, S. Pokorna, S. Pullanchery, M. Kohagen, P. Jurkiewicz, M. Hof, P. Jungwirth, P.S. Cremer, L. Cwiklik, The complex nature of calcium cation interactions with phospholipid bilayers, *Scientific Reports*, 6 (2016) 38035.
- [18] J.F. Nagle, S. Tristram-Nagle, Structure of lipid bilayers, *Biochim Biophys Acta*, 1469 (2000) 159-195.
- [19] H.P. Wacklin, Neutron reflection from supported lipid membranes, *Current Opinion in Colloid & Interface Science*, 15 (2010) 445-454.
- [20] T.K. Lind, M. Cardenas, Understanding the formation of supported lipid bilayers via vesicle fusion- A case that exemplifies the need for the complementary method approach (Review), *Biointerphases*, 11 (2016) 020801.
- [21] D. Di Silvio, M. Maccarini, R. Parker, A. Mackie, G. Fragneto, F. Baldelli Bombelli, The effect of the protein corona on the interaction between nanoparticles and lipid bilayers, *Journal of Colloid and Interface Science*, 504 (2017) 741-750.
- [22] K.L. Browning, T.K. Lind, S. Maric, S. Malekhaiat-Häffner, G.N. Fredrikson, E. Bengtsson, M. Malmsten, M. Cárdenas, Human Lipoproteins at Model Cell Membranes: Effect of Lipoprotein Class on Lipid Exchange, *Scientific Reports*, 7 (2017) 7478.
- [23] T. Soranzo, D.K. Martin, J.-L. Lenormand, E.B. Watkins, Coupling neutron reflectivity with cell-free protein synthesis to probe membrane protein structure in supported bilayers, *Scientific Reports*, 7 (2017) 3399.
- [24] M.K. Baumann, E. Amstad, A. Mashaghi, M. Textor, E. Reimhult, Characterization of supported lipid bilayers incorporating the phosphoinositides phosphatidylinositol 4,5-bisphosphate and phosphoinositol-3,4,5-triphosphate by complementary techniques, *Biointerphases*, 5 (2010) 114-119.

- [25] M.K. Baumann, M.J. Swann, M. Textor, E. Reimhult, Pleckstrin homology-phospholipase C-delta1 interaction with phosphatidylinositol 4,5-bisphosphate containing supported lipid bilayers monitored in situ with dual polarization interferometry, *Anal Chem*, 83 (2011) 6267-6274.
- [26] E.L. Wu, Y.F. Qi, K.C. Song, J.B. Klauda, W. Im, Preferred Orientations of Phosphoinositides in Bilayers and Their Implications in Protein Recognition Mechanisms, *J Phys Chem B*, 118 (2014) 4315-4325.
- [27] F. Foglia, M.J. Lawrence, D.J. Barlow, Studies of model biological and bio-mimetic membrane structure: Reflectivity vs diffraction, a critical comparison, *Current Opinion in Colloid & Interface Science*, 20 (2015) 235-243.
- [28] A.S. Cans, F. Hook, O. Shupliakov, A.G. Ewing, P.S. Eriksson, L. Brodin, O. Orwar, Measurement of the dynamics of exocytosis and vesicle retrieval at cell populations using a quartz crystal microbalance, *Anal Chem*, 73 (2001) 5805-5811.
- [29] F. Höök, Development of a Novel QCM Technique for Protein Adsorption Studies, Department of Applied Physics, Chalmers University of Technology, Göteborg, 1997.
- [30] R.A. Campbell, H.P. Wacklin, I. Sutton, R. Cubitt, G. Fragneto, FIGARO: The new horizontal neutron reflectometer at the ILL, *Eur Phys J Plus*, 126 (2011).
- [31] L. Braun, M. Uhlig, R. von Klitzing, R.A. Campbell, Polymers and surfactants at fluid interfaces studied with specular neutron reflectometry, *Adv Colloid Interfac*, 247 (2017) 130-148.
- [32] R. Cubitt, G. Fragneto, D17: the new reflectometer at the ILL, *Appl Phys a-Mater*, 74 (2002) S329-S331.
- [33] G. Fragneto-Cusani, Neutron reflectivity at the solid/liquid interface: examples of applications in biophysics, *J Phys-Condens Mat*, 13 (2001) 4973-4989.
- [34] <http://sourceforge.net/projects/rscl/>.
- [35] M.B. Emil Wolf, Principles of Optics, Pergamon Press 1970.
- [36] Y. Gerelli, Aurore: new software for neutron reflectivity data analysis, *Journal of Applied Crystallography*, 49 (2016) 330-339.
- [37] M. Maccarini, E.B. Watkins, B. Stidder, J.-P. Alcaraz, B.A. Cornell, D.K. Martin, Nanostructural determination of a lipid bilayer tethered to a gold substrate, *The European Physical Journal E*, 39 (2016) 123.
- [38] R.S. Armen, O.D. Uitto, S.E. Feller, Phospholipid component volumes: determination and application to bilayer structure calculations, *Biophys J*, 75 (1998) 734-744.
- [39] N. Kučerka, S. Tristram-Nagle, J.F. Nagle, Structure of Fully Hydrated Fluid Phase Lipid Bilayers with Monounsaturated Chains, *The Journal of Membrane Biology*, 208 (2006) 193-202.
- [40] V. Rondelli, P. Brocca, N. Tranquilli, G. Fragneto, E. Del Favero, L. Cantu, Building a biomimetic membrane for neutron reflectivity investigation: Complexity, asymmetry and contrast, *Biophys Chem*, 229 (2017) 135-141.
- [41] C.A. Keller, B. Kasemo, Surface specific kinetics of lipid vesicle adsorption measured with a quartz crystal microbalance, *Biophys J*, 75 (1998) 1397-1402.
- [42] F. Höök, B. Kasemo, T. Nylander, C. Fant, K. Sott, H. Elwing, Variations in Coupled Water, Viscoelastic Properties, and Film Thickness of a Mefp-1 Protein Film during Adsorption and Cross-Linking: A Quartz Crystal Microbalance with Dissipation Monitoring, Ellipsometry, and Surface Plasmon Resonance Study, *Analytical Chemistry*, 73 (2001) 5796-5804.
- [43] S. Bobone, Y. Gerelli, M. De Zotti, G. Bocchinfuso, A. Farrotti, B. Orioni, F. Sebastiani, E. Latter, J. Penfold, R. Senesi, F. Formaggio, A. Palleschi, C. Toniolo, G. Fragneto, L. Stella, Membrane thickness and the mechanism of action of the short peptaibol trichogin GA IV, *Biochim Biophys Acta*, 1828 (2013) 1013-1024.
- [44] A. Akesson, T. Lind, N. Ehrlich, D. Stamou, H. Wacklin, M. Cardenas, Composition and structure of mixed phospholipid supported bilayers formed by POPC and DPPC, *Soft Matter*, 8 (2012) 5658-5665.
- [45] Anton P. Le Brun, Cathryn L. Haigh, Simon C. Drew, M. James, Martin P. Boland, Steven J. Collins, Neutron Reflectometry Studies Define Prion Protein N-terminal Peptide Membrane Binding, *Biophys J*, 107 (2014) 2313-2324.

- [46] H.P. Wacklin, F. Tiberg, G. Fragneto, R.K. Thomas, Distribution of reaction products in phospholipase A2 hydrolysis, *Biochim Biophys Acta*, 1768 (2007) 1036-1049.
- [47] N.R. Yepuri, T.A. Darwish, A.M. Krause-Heuer, A.E. Leung, R. Delhom, H.P. Wacklin, P.J. Holden, Synthesis of Perdeuterated 1-Palmitoyl-2-oleoyl-sn-glycero-3-phosphocholine ([D82]POPC) and Characterisation of Its Lipid Bilayer Membrane Structure by Neutron Reflectometry, *ChemPlusChem*, 81 (2015) 315-321.
- [48] J. Lu, A.P. Le Brun, S.H. Chow, T. Shiota, B. Wang, T.W. Lin, G.S. Liu, H.H. Shen, Defining the structural characteristics of annexin V binding to a mimetic apoptotic membrane, *Eur Biophys J*, 44 (2015) 697-708.
- [49] D.P. Chang, A.P. Dabkowska, R.A. Campbell, M. Wadsater, J. Barauskas, F. Tiberg, T. Nylander, Interfacial properties of POPC/GDO liquid crystalline nanoparticles deposited on anionic and cationic silica surfaces, *Phys Chem Chem Phys*, 18 (2016) 26630-26642.
- [50] R. Eells, M. Barros, K.M. Scott, I. Karageorgos, F. Heinrich, M. Losche, Structural characterization of membrane-bound human immunodeficiency virus-1 Gag matrix with neutron reflectometry, *Biointerphases*, 12 (2017) 02D408.
- [51] J.P. Bradshaw, R.J. Bushby, C.C. Giles, M.R. Saunders, Orientation of the headgroup of phosphatidylinositol in a model biomembrane as determined by neutron diffraction, *Biochemistry*, 38 (1999) 8393-8401.
- [52] Z. Li, R.M. Venable, L.A. Rogers, D. Murray, R.W. Pastor, Molecular Dynamics Simulations of PIP2 and PIP3 in Lipid Bilayers: Determination of Ring Orientation, and the Effects of Surface Roughness on a Poisson-Boltzmann Description, *Biophys J*, 97 (2009) 155-163.
- [53] H.P. Wacklin, Composition and Asymmetry in Supported Membranes Formed by Vesicle Fusion, *Langmuir*, 27 (2011) 7698-7707.
- [54] J. Larsen, N.S. Hatzakis, D. Stamou, Observation of inhomogeneity in the lipid composition of individual nanoscale liposomes, *J Am Chem Soc*, 133 (2011) 10685-10687.